SCIENTIFIC REPORTS

OPEN

SUBJECT AREAS:
APPLIED PHYSICS
MAGNETIC PROPERTIES AND MATERIALS

Received
13 January 2014

Accepted
14 March 2014

Published
1 April 2014

Correspondence and requests for materials should be addressed to J.M.H. (juh34@psu.edu) or C.W.N. (cwnan@tsinghua.edu.cn)

* These authors contributed equally to this work.

Effect of strain on voltage-controlled magnetism in $BiFeO_3$-based heterostructures

J. J. Wang[1]*, J. M. Hu[1,2]*, T. N. Yang[2], M. Feng[1], J. X. Zhang[3], L. Q. Chen[1,2] & C. W. Nan[1]

[1]State Key Lab of New Ceramics and Fine Processing, School of Materials Science and Engineering, Tsinghua University, Beijing, 100084, China, [2]Department of Materials Science and Engineering, The Pennsylvania State University, University Park, Pennsylvania, 16802, USA, [3]Department of Physics, Beijing Normal University, Beijing, 100875, China.

Voltage-modulated magnetism in magnetic/$BiFeO_3$ heterostructures can be driven by a combination of the intrinsic ferroelectric-antiferromagnetic coupling in $BiFeO_3$ and the antiferromagnetic-ferromagnetic exchange interaction across the heterointerface. However, ferroelectric $BiFeO_3$ film is also ferroelastic, thus it is possible to generate voltage-induced strain in $BiFeO_3$ that could be applied onto the magnetic layer across the heterointerface and modulate magnetism through magnetoelastic coupling. Here, we investigated, using phase-field simulations, the role of strain in voltage-controlled magnetism for these $BiFeO_3$-based heterostructures. It is predicted, under certain condition, coexistence of strain and exchange interaction will result in a pure voltage-driven 180° magnetization reversal in $BiFeO_3$-based heterostructures.

It is accepted that voltage-modulated magnetism in magnetic/$BiFeO_3$ (BFO) layered heterostructures is based on a combination of intrinsic coupling between the coexisted ferroelectric and antiferromagnetic orders in BFO, and the antiferromagnetic-magnetic exchange interaction across the heterointerface[1–4]. However, ferroelectric BFO film, if not fully clamped by substrate, would generate voltage-induced strains that could be transferred to the magnetic thin film across the heterointerface and modulate magnetism together with exchange interaction through magnetoelastic coupling. Influence of this strain on voltage-modulated magnetism in BFO-based heterostructures has remained largely unexplored since raised by Mathur[5], though a giant voltage-induced strain of over 5% has later been observed in BFO thin films with mixed rhombohedral and tetragonal phases[6,7].

In this article, we explore how strain affects the voltage-modulated magnetism in BFO-based heterostructures by taking the $Co_{0.9}Fe_{0.1}$(CoFe)/BFO thin-film heterostructure as an example. (001) BFO thin films were grown on (110) $DyScO_3$ substrate, exhibiting two-variant ferroelectric domains with 71° wall due to anisotropic film-substrate misfit strains[8]. In particular, the magnetic domain patterns in the top CoFe film almost copy the in-plane projection patterns of the ferroelectric domains at the BFO surface[2,9]. Such magnetic domain pattern is induced by an effective magnetic field from the canted magnetic moment $\mathbf{M}_c$ in BFO via Dzyaloshinskii-Moriya (DM) exchange interaction[10,11], namely, $\mathbf{H}_{DM}$-field. The direction of $\mathbf{H}_{DM}$-field (also $\mathbf{M}_c$) is perpendicular to the plane of the polarization $\mathbf{P}$ and the antiferromagnetic axis $\mathbf{L}$[12,13], i.e., $\mathbf{H}_{DM}=\mathbf{P}\times\mathbf{L}$, resulting in a non-uniform $\mathbf{H}_{DM}$-field distribution based on the two-variant 71° ferroelectric domains. In this case, when electrically rearranging ferroelectric domain configuration to switch the in-plane net polarization in BFO by 180°, rotation of $\mathbf{H}_{DM}$-field within individual ferroelectric domain could lead to an overall 180° switching of the in-plane net magnetization[2] in CoFe. Detailed experimental analysis[14] reveals that the $\mathbf{H}_{DM}$-field ($\mathbf{M}_c$) lies along the $[\bar{1}\,\bar{1}\,2]$and $[\bar{1}1\bar{2}]$ directions corresponding to the $[\bar{1}\,\bar{1}1]$ and $[\bar{1}11]$ polarizations, while along the $[1\bar{1}2]$and $[11\bar{2}]$ directions corresponding to the $[1\bar{1}1]$ and $[111]$ polarizations, respectively (figure 1a).

Furthermore, the first few unit cells at the BFO thin film surface would become stress-free when the thickness of the BFO film was above a certain critical value [t_c ~70 nm for the BFO films grown on $DyScO_3$(DSO) substrate[15,16]] to allow the presence of lattice defects such as dislocation (figure 1b). In this case, sizable and non-uniform strain can be generated associated with local non-180° ferroelectric polarization (i.e., ferroelastic) switching under an electric-field. The strain can be further transferred to the top magnetic thin film across the interface and modulate the magnetic domain structure locally via magnetoelastic coupling[17]. Transfer of such non-uniform strain has recently been demonstrated in $BaTiO_3$ single crystal-based heterostructues[18-21], which exhibit a similar one-to-one domain pattern match between magnetic thin film and ferroelectric $BaTiO_3$ under-

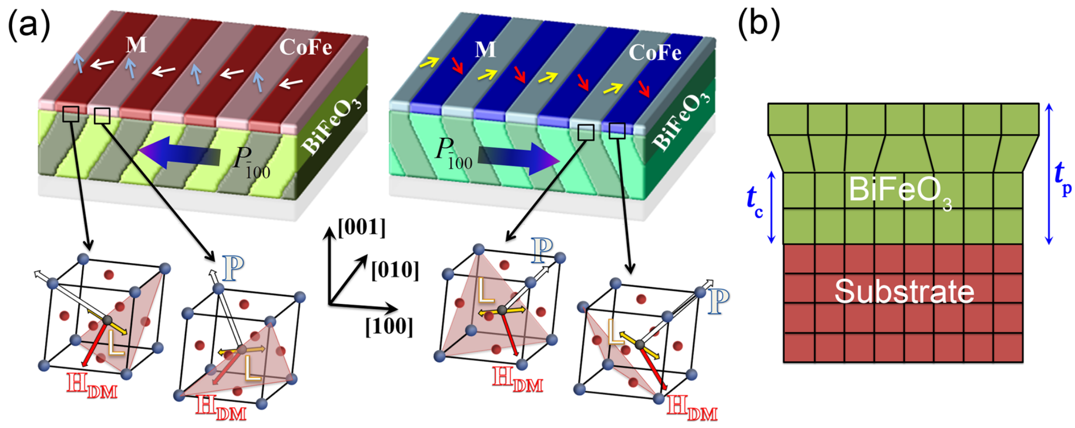

Figure 1 | Voltage-controlled magnetism in CoFe/BiFeO$_3$ heterostructure. (a) Locally coupled magnetic and ferroelectric domains in the $Co_{0.9}Fe_{0.1}$(CoFe)/$BiFeO_3$(BFO) heterostructure reproduced by phase-field model (the first row), based on electric-field switching of the interfacial exchange coupling field $\mathbf{H}_{DM}$ which is perpendicular to the plane of electric polarization **P** and the antiferromagnetic axis **L** in BFO (the second row). The slim arrows indicate orientations of local magnetization vectors. (b) Schematic of an epitaxial BFO film with partially relaxed substrate clamping when the film thickness t_p exceeds the critical value t_c for the generation of interfacial dislocations.

neath. Particularly, it was proposed that[22] such non-uniform ferroelastic strain transfer alone could drive a 180° in-plane net magnetization reversal similarly to the non-uniform H_{DM}-field driven reversal shown in figure 1a. These similarities thus raise one interesting question for BFO-based heterostructures: what role does the non-uniform strain in BFO play in the electric-field induced magnetization reversal? A phase-field[23,24] model is developed herein (see Method section) to address this question, and illustrate new possibility in electric-field-controlled magnetism under coexistence of non-uniform H_{DM}-field and non-uniform strain.

Results

In-plane net magnetization reversal purely by H_{DM}-field. We first examine the influence of the interfacial H_{DM}-field on the electric-field driven magnetization reversal in the CoFe/BFO heterostructure. If the electric-field applied along the [100] direction (E_{100}) exceeds the coercive field of BFO (E_c), the initial alternating $[\bar{1}\bar{1}1]$and $[\bar{1}11]$ ferroelectric domains would switch by 71° to the $[1\bar{1}1]$ and [111] domains, respectively, during which the polarization vectors would always keep a *head to tail* configuration (see figure 2a) to reduce the electrostatic energy. This leads to a full reversal of the average polarization along the [100] direction (i.e., P_{100}), as illustrated by the simulated ferroelectric hysteresis loop in figure 2c. Note that individual ferroelectric domain under a certain E_{100} results in one unique local H_{DM}-field distribution [Eq. (11)]. Correspondingly, figure 2b presents the in-plane projections of the H_{DM}-field, e.g., an initial configuration of *head to tail* in-plane $[\bar{1}\bar{1}0]$ and $[\bar{1}10]$orientations. The induced local magnetization distributions (*viz.* domain structures) in the CoFe film are almost identical to those of in-plane H_{DM}-field (not shown here for simplicity), while both distributions are essentially the same as the in-plane projections of the ferroelectric domains and thereby accounts for the domain pattern transfer between the CoFe and BFO films[2]. Furthermore, a full reversal of the net [100] magnetization (M_{100}) in the CoFe film occurs when reversing the average in-plane H_{DM} field along the [100] direction ($\mathbf{H}_{DM}^{100}$) with an electric-field, as shown by their electric-field switching loops in figure 2e and 2d, respectively. The magnitude of the total H_{DM} field [i.e., h_{DM}^0, see Eqs. (11) and (12) in the Method section] is taken as 100 Oe based on a relevant experimental measurment[9].

It is worth noting that such net magnetization reversal may not be triggered if the h_{DM}^0 was too small, because the striped magnetic domains cannot be stabilized unless h_{DM}^0 exceeds 35 Oe (see figure 3a), where the influence of strains is not incorporated (λ_s=0). As it can be seen, once the striped domains form at 35 Oe, the net in-plane magnetization can then be reversed, i.e., the normalized magnetization M_{100}/M_s changes from −0.7 to about 0.7, by changing the polarity of the net in-plane polarization. Simulated magnetic and ferroelectric domain structures at h_{DM}^0 =6 Oe and 100 Oe are illustrated in the inset of figure 3a. We argue that the critical h_{DM}^0 value for net magnetization reversal should be strongly dependent on the coercive field of the magnetic thin film, because influence of H_{DM}-field is equivalent to an external non-uniform magnetic field [Eq. (9)].

Full magnetization reversal driven by both H_{DM}-field and strain. Figure 3b shows the M_{100}/M_s variations as a function of h_{DM}^0 before (the upper panel) and after (the lower panel) reversing the net in-plane polarization, driven by both non-uniform H_{DM}-field and non-uniform ferroelastic strain. Strain distributions before and after polarization reversal are plotted in figure 3c, with an alternating distribution of ±0.6% [also see Eq. (4a)]. Of interest, the magnetic striped domains can be stabilized during the growth of CoFe film by the growth-induced strains [see Eq. 4(b)] imposed by the striped ferroelectric (also ferroelastic) domain pattern at the BFO surface even when h_{DM}^0 =0 (i.e., no exchange interaction but sole strain effect, see figure 3b). However, these striped domains cannot be switched to achieve an in-plane net magnetization reversal when h_{DM}^0 is small (weak exchange interaction). For example, at h_{DM}^0 =6 Oe, the striped domains only demonstrate a change in pattern periodicity (see corresponding domain structures in the inset of figure 3b) when reversing in-plane polarization. Thus, although non-uniform ferroelastic strain contributes to the stabilization of the domain stripes, it alone cannot trigger the net magnetization reversal. On the contrary, this strain could even suppress the reversal compared to the case purely driven by H_{DM}-field (figure 3a), as demonstrated by (*i*) the enhancement of the critical value of h_{DM}^0 from 35 Oe to 45 Oe (see the solid line in figure 3b), and (*ii*) the different magnetic domain stripes at h_{DM}^0 =6 Oe (prevailing strain effect) and 1000 Oe (prevailing exchange interaction) with the same FE domain patterns underneath (i.e., both are before electric-field poling, see the upper panel of figure 3b).

These counteractive non-uniform H_{DM}-field and non-uniform strain can, however, be exploited to achieve a full rather than net magnetization reversal. As shown in figure 3b, the magnetic striped domains are straightened out to form a uniform single domain when

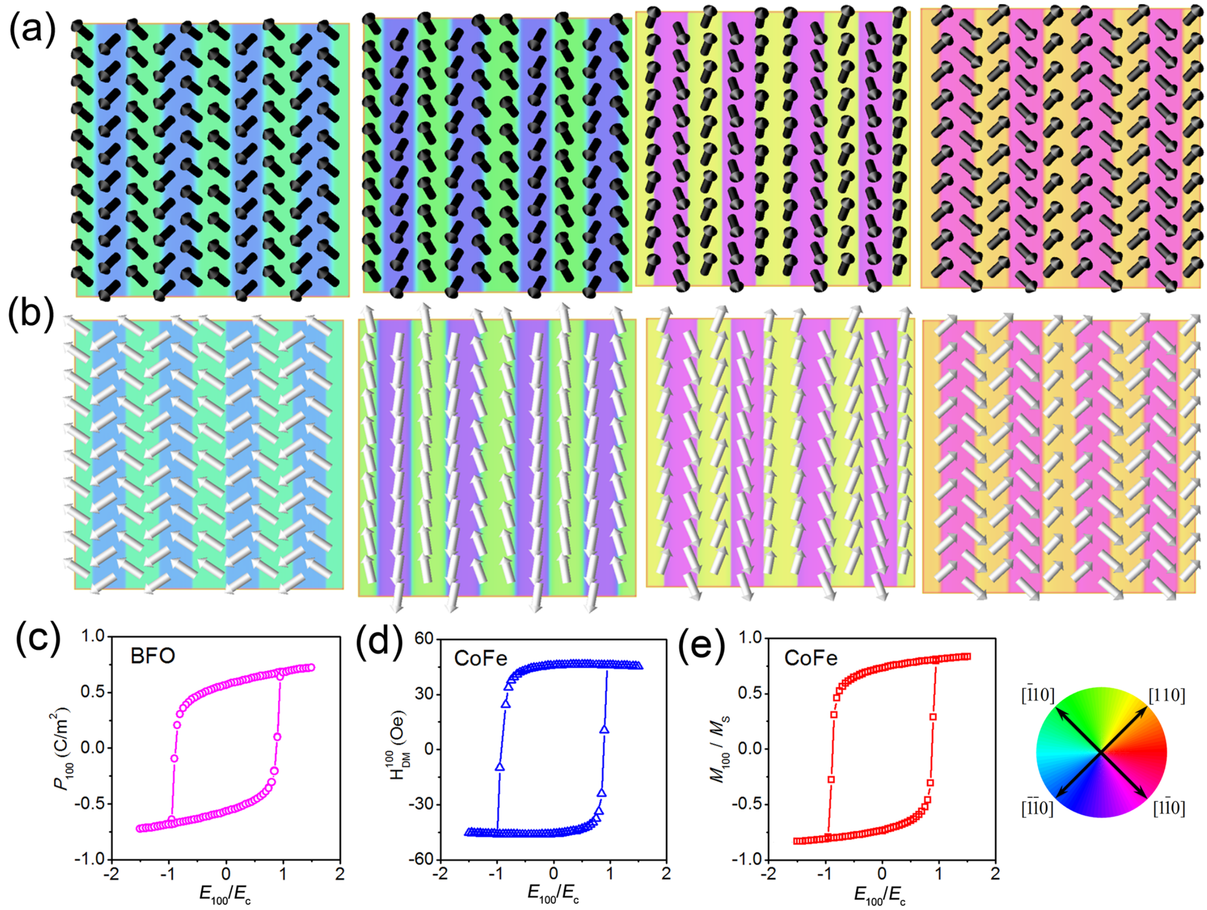

Figure 2 | In-plane net magnetization reversal via electric-field switchable $\mathbf{H}_{DM}$-field. In-plane electric-field (E_{100}/E_c=1) induced dynamic changes in (a) the local distributions of polarization (top view) in the two-domain-variant BFO film, and (b) the in-plane projections of the $\mathbf{H}_{DM}$-field (the same for the local magnetization). The background color indicates the orientation of the local polarization/$\mathbf{H}_{DM}$/magnetization field (see the color wheel). Electric-field switching loops of average (c) polarization, (d) in-plane $\mathbf{H}_{DM}$ field, and (e) magnetization along the [100] direction. E_c represents the coercive field of the BFO film.

h^0_{DM} is about 500 Oe. We attribute this to the almost equal contributions from the competing strain effect and exchange interaction at this point. Indeed, taking the coupled magnetic and ferroelectric domain structures at h^0_{DM} =0 Oe as the reference, the changes in magnetic free energy induced by strain and $\mathbf{H}_{DM}$-field are 8.26 × 10^4 J/m^3 and −7.95 × 10^4 J/m^3, respectively, at h^0_{DM} =500 Oe. Furthermore, a full 180° magnetization reversal takes place when reversing the in-plane polarization (see corresponding domain structures in figure 3b), which should promise higher application potential for low-power memory applications[25,26] than the average magnetization reversal in striped multi-domain. Further simulations show that the range of h^0_{DM} required for such voltage-driven 180° magnetization reversal is from 393 Oe to 778 Oe, whereas the rest h^0_{DM} values that are over 45 Oe only lead to a net magnetization reversal, in which the contribution form $\mathbf{H}_{DM}$-field is enough to trigger magnetization reversal but much smaller/larger than contribution from strain. Particularly, the range of h^0_{DM} for 180° reversal can be tuned by engineering the saturation magnetostriction coefficient λ_s (e.g., by using different magnets) and/or the magnitude of ferroelastic strains [e.g., by tuning polarization, see Eq. (4a)]. Detailed analysis can be found in Supplemental materials S1.

Dynamics of magnetic domain switching. So far three different voltage-induced magnetic domain switching paths has been observed under the coexistence of $\mathbf{H}_{DM}$-field and strain, including the change in domain pattern periodicity (pattern exchange) when $\mathbf{H}_{DM}$-field is weak or absent (h^0_{DM}< 45 Oe), the full magnetization reversal when contributions from $\mathbf{H}_{DM}$-field and strain are comparable (393 Oe < h^0_{DM} < 778 Oe), and the net magnetization reversal for the remaining values of h^0_{DM}. To unravel the underlying physics, we track the time-dependent changes in the sum of the magnetostatic and exchange energy (i.e., F_{ms} + F_{exch}) for these different paths (figure 4), and their local magnetic vector distributions at various time stages are shown in Supplemental Materials S2. For the net magnetization reversal at h^0_{DM} =1000 Oe, an energy barrier is surmounted during its initial stages (<0.04 ns), whereas for the change in domain pattern periodicity at h^0_{DM} =6 Oe, a lower energy path is present throughout the evolution. Given the almost identical energy states between these striped domains with opposite net magnetization (i.e., pattern exchange and net reversal in figure 4), and also given their similar energy oscillation trends after surmounting the energy barrier, it can be concluded that the energy barrier can only be overcome by the unidirectional $\mathbf{H}_{DM}$-field rather than the uniaxial strain. In particular, for the full magnetization reversal at h^0_{DM} =500 Oe, the counteraction between $\mathbf{H}_{DM}$-field and strain leads to the lowest energy state before and after switching, however, an energy barrier still needs to be surmounted to complete the reversal.

Discussion

Voltage-controlled magnetism in magnetic/$BiFeO_3$ heterostructures is a complex process with multiple underlying mechanisms, depend-

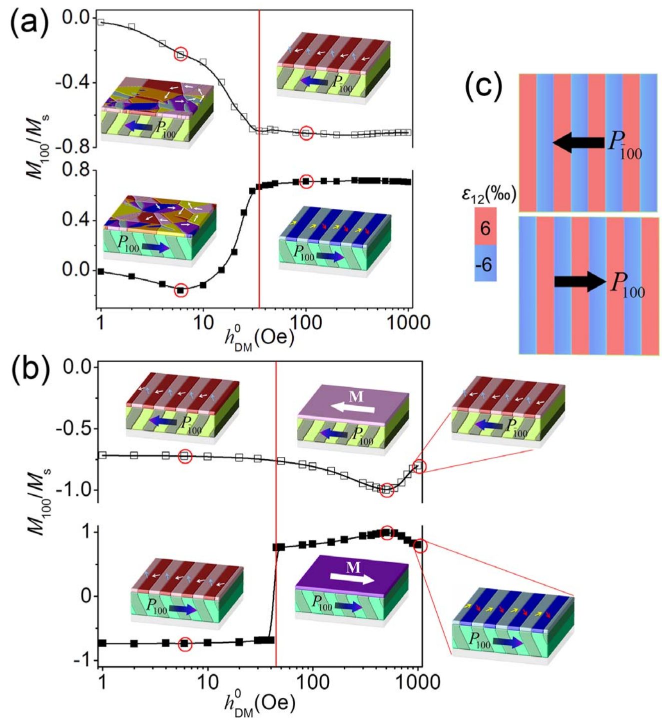

Figure 3 | Effects of H_{DM}-field and strain on voltage-induced magnetic domain switching. Variations on M_{100}/M_s (the normalized magnetization along the [100] direction) as a function of h^0_{DM} (the magnitude of the $\mathbf{H}_{DM}$-field) before and after reversing the in-plane average polarization from P_{100} to $P_{\bar{1}00}$ in the CoFe/BFO heterostructure, driven by (a) only $\mathbf{H}_{DM}$-field, and (b) $\mathbf{H}_{DM}$-field together with ferroelastic strain. The insets are magnetic and ferroelectric domain structures at $h^0_{DM} = 6$ Oe and 100 Oe in (a), and the 6 Oe, 500 Oe, and 1000 Oe in (b). The slim arrows indicate the orientations of local magnetization vectors. (c) Distribution of the non-uniform ferroelastic strain arising from the ferroelectric domains at the BFO surface before and after polarization reversal.

ing on the size of such heterostructures[27]. In the present article, our focus has been put on the effects of both ferroelastic strains and DM exchange interaction in the CoFe/BiFeO$_3$ heterostructures currently investigated. Besides these effects, the modulation of magnetism could also be contributed by the voltage-induced changes in interface charge densities[28,29], and/or interface orbital configuration (e.g., via Fe-O hybridization, refs. 30,31). Such interface effects would become more remarkable as the thickness of the CoFe film (2.5 nm herein) further decreases[32]. On the other hand, further decrease in the lateral size of the heterostructures may allow us to study the complex interplay among strain, exchange interaction, and possibly the charge/orbital effect in ferroic single-domains. This is not only fundamentally interesting, but also important for the design of high-density magnetoelectric devices[25,26]. The model established herein could provide a good starting point for the further study of these issues.

In summary, a phase-field model has been developed to understand how strain affects the voltage-modulated magnetism in BFO-based heterostructures. The model is validated by reproducing the experimentally observed voltage-driven in-plane net magnetization reversal in a CoFe/BFO heterostructure[2] driven by non-uniform $\mathbf{H}_{DM}$-field. Then we evaluate the stable magnetic and ferroelectric domain structures by adding the influence of the non-uniform ferroelastic strain that arises from the ferroelectric domain patterns at the BFO surface. Under such coexistence of $\mathbf{H}_{DM}$-field and strain, three different magnetic domain switching paths are discovered depending on the magnitude of the $\mathbf{H}_{DM}$-field, including a full 180° reversal of uniform magnetization when contributions from

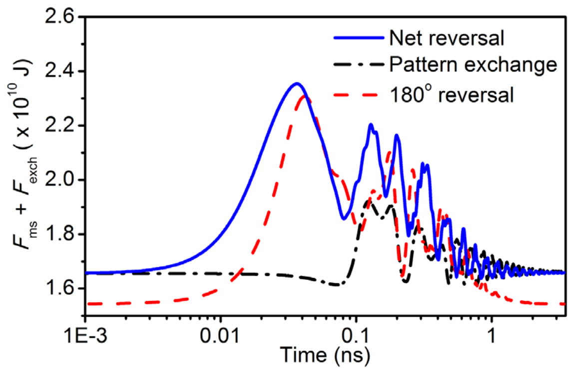

Figure 4 | Free energy analysis for different voltage-induced magnetic domain switching paths. Time-dependent changes in the sum of magnetostatic and exchange energy for three different voltage-induced magnetic domain switching in CoFe/BFO heterostructures, driven by both non-uniform $\mathbf{H}_{DM}$-field and non-uniform strain. The magnitudes of $\mathbf{H}_{DM}$-field (h^0_{DM}) are taken as 6 Oe, 500 Oe, and 1000 Oe for pattern exchange, net magnetization reversal, and 180° full magnetization reversal, respectively.

$\mathbf{H}_{DM}$-filed and strain are comparable. Analysis on magnetic domain switching dynamics demonstrates the lowest energy state for such full magnetization reversal, as well as the decisive role of $\mathbf{H}_{DM}$-field for both full and net magnetization reversals.

Methods

Phase-field model. In phase field approach, the magnetic and ferroelectric domain structures are described by the spatial distributions of the local magnetization vector $\mathbf{M}=M_S(m_1,m_2,m_3)$ and local polarization vector $\mathbf{P}=(P_1,P_2,P_3)$, respectively, where M_S and m_i (i=1,2,3) represent the saturation magnetization and the direction cosine[33].

The temporal evolution of the ferroelectric domain structure in (001)-oriented BFO thin films is governed by the time-dependent Landau-Ginzburg (TDGL) equation[34], i.e.,

$$\frac{\partial P_i(\mathbf{r},t)}{\partial t} = -L\frac{\delta F_P}{\delta P_i(\mathbf{r},t)}, \tag{1}$$

where L is a kinetic coefficient that is related to the domain wall mobility and F_P is the total free energy of the FE layer, which can be expressed as,

$$F_P = \iiint_{V_P} \left(f_{bulk} + f^{P}_{elastic} + f_{electric} + f_{grad}\right) dV, \tag{2}$$

here f_{bulk}, $f^P_{elastic}$, $f_{electric}$, and f_{grad} indicate the densities of bulk free energy, elastic energy, electrostatic energy, and gradient energy of the BFO, respectively, with V_P representing the volume of the ferroelectric layer in the heterostructure. The mathematical expressions for the f_{bulk}, f_{grad}, and $f_{electric}$ of the BFO (001) thin films are described in literature[35]. Corresponding to the local in-plane electric-fields applied across the CoFe/BFO heterostructure via planar poling electrodes[2], the electrostatic energy density $f_{electric}$ is obtained under a short-circuit boundary condition[36].

The elastic energy density $f^P_{elastic}$ is calculated as,

$$f^P_{elastic} = \frac{1}{2}c^P_{ijkl}e_{ij}(\mathbf{r})e_{kl}(\mathbf{r}) = \frac{1}{2}c^P_{ijkl}\left[\varepsilon_{ij}(\mathbf{r}) - \varepsilon^{0-P}_{ij}(\mathbf{r})\right]\left[\varepsilon_{kl}(\mathbf{r}) - \varepsilon^{0-P}_{kl}(\mathbf{r})\right], \tag{3}$$

where c^P_{ijkl} is the elastic stiffness tensor of the BFO and $e_{ij}(\mathbf{r})$ the position-dependent elastic strain; $\varepsilon_{ij}(\mathbf{r})$ is the total strain and $\varepsilon^{0-P}_{ij}(\mathbf{r})$ is the spontaneous (stress-free) strain of the BFO arising from the electrostrictive effect, i.e., $\varepsilon^{0-P}_{ij}(\mathbf{r}) = Q_{ijkl}P_k(\mathbf{r})P_l(\mathbf{r})$ (i,j,k,l=1,2,3,4), where Q_{ijkl} is the electrostrictive coefficient tensor. Following Khachaturyan's elastic theory[37], the total strain $\varepsilon_{ij}(\mathbf{r})$ can be expressed as the sum of homogeneous and heterogeneous strains, i.e. $\varepsilon_{ij}(\mathbf{r}) = \overline{\varepsilon_{ij}} + \delta\varepsilon_{ij}(\mathbf{r})$. Among them, the heterogeneous strain $\delta\varepsilon_{ij}(\mathbf{r})$ does not cause any macroscopic deformation in a sample, i.e., $\int \delta\varepsilon_{ij}(\mathrm{r})dV = 0$, and can be calculated as $\delta\varepsilon_{ij}(\mathbf{r}) = \left[\partial u_i(\mathbf{r})/\partial x_j + \partial u_j(\mathbf{r})/\partial x_i\right]/2$, where $u_i(\mathbf{r})$ is the displacement.

The homogeneous strain $\overline{\varepsilon_{ij}}$ represents the macroscopic deformation, whose in-plane components equal the film/substrate mismatch strain e^s_{ij} if the BFO (001) thin films were fully constrained by the DSO (110) substrate, i.e., $\overline{\varepsilon_{11}} = e^s_{11} = -0.35\%$, $\overline{\varepsilon_{22}} = e^s_{22} = -0.48\%$, and $\overline{\varepsilon_{12}} = \overline{\varepsilon_{21}} = 0$. The mechanical equilibrium equation, i.e., $\partial\sigma_{ij}/\partial x_i = \partial\left(\partial f^P_{elastic}/\partial\overline{\varepsilon_{ij}}\right)/\partial x_i = 0$, is then solved by taking $\sigma_{13}=\sigma_{23}=\sigma_{33}=0$[38]. It is noteworthy that such anisotropic biaxial in-plane strains can reduce the ferroelectric domain variants of the rhombohedral BFO from eight to two[8], leading to the unique two-variant striped domains with 71° walls as reconstructed in figure 1a. Particularly, in a partly relaxed BFO thin film (figure 1b), a non-uniform ferroelastic strain ε_{ij}^{FS} could be generated across the first few stress-free unit cells of individual ferroelectric domain, which can be expressed as,

$$\varepsilon_{ij}^{FS} = \frac{1}{t_s}\int_{t_s} Q_{ijkl}P_kP_l dz. \tag{4a}$$

Here $t_s(=t_p\text{-}t_c)$ denotes the thickness of the stress-free unit cells at the BFO film surface (see figure 1b), which is approximated to be 40 nm by taking the total thickness t_p of BFO as 110 nm[39].

Corresponding to the two-variant FE domains at the BFO surface, a two-variant striped strain distribution with alternating ±0.6% can be derived. Such non-uniform strain ε_{ij}^{FS} would further be transferred, at least partially[18], to the upper CoFe film that has a much smaller thickness (t_m ~2.5 nm, ref. 2) than t_s. Note that the two-variant striped domains in the BFO film should still emerge at the thickness t_p of 110 nm as observed in experiments[39], though the possible interfacial dislocations would somewhat release the anisotropic mismatch strains from the orthorhombic DSO substrate. Nevertheless, even the fully constrained BFO thin films with striped domains can impose structural strains on the upper magnetic thin film during its growth,[33] similarly to those observed in magnetic/$BaTiO_3$ heterostructures.[18,19] Thus, the average growth-induced strain affects the domain structure of the as-grown magnetic thin film together with the interfacial $\mathbf{H}_{DM}$ field, which can be expressed as,

$$\varepsilon_{ij}^{growth} = \frac{1}{t_p}\int_{t_p} Q_{ijkl}P_k^S P_l^S dz, \tag{4b}$$

where P_k^S is the spontaneous (or remnant) polarizations under zero external electric fields. Accordingly, when applying an electric-field to the BFO film, the resultant polarization switching would change spatial distributions of both the $\mathbf{H}_{DM}(=\mathbf{P}\times\mathbf{L})$ field and the strain ε_{ij}^{FS} [Eq. (4a)] at the interface.

Magnetic domain structures of the CoFe film will then evolve driven by these non-uniform $\mathbf{H}_{DM}$ field and non-uniform ε_{ij}^{FS} (or the $\varepsilon_{ij}^{growth}$ for simulating the domain structures of as-grown CoFe film), and can be described by the Landau-Lifshitz-Gilbert (LLG) equation, i.e.,

$$\left(1+\alpha^2\right)\frac{\partial \mathbf{M}}{\partial \tau} = -\gamma_0 \mathbf{M}\times\mathbf{H}_{\text{eff}} - \frac{\gamma_0\alpha}{M_S}\mathbf{M}\times(\mathbf{M}\times\mathbf{H}_{\text{eff}}). \tag{5}$$

Here γ_0 and α are the gyromagnetic ratio (taken as -2.2×10^5 m·A^{-1}·s^{-1} from ref. 40) and the Gilbert damping constant (~0.01 from ref.41), respectively, whereby the real time step ΔT (~0.06 ps) for the magnetic domain evolution can be determined by $\Delta T = \tau\left(1+\alpha^2\right)/(\gamma_0 M_S)$ with $\Delta\tau=0.02$. $\mathbf{H}_{\text{eff}}$ is the effective magnetic field, given as $\mathbf{H}_{\text{eff}} = -(1/\mu_0)(\delta F_m/\delta\mathbf{M})$, with μ_0 denoting the vacuum permeability and F_m the total free energy of the CoFe layer. The F_m is formulated as,

$$F_M = \iiint_V \left(f_{\text{anis}} + f_{\text{exch}} + f_{\text{ms}} + f_H + f_{\text{elastic}}^m\right)dV, \tag{6}$$

where f_{anis}, f_{exch}, f_{ms}, f_H, and f_{elastic}^m are the magnetocrystalline anisotropy energy density, exchange energy density, magnetostatic energy density, the $\mathbf{H}_{DM}$-field energy density, and elastic energy density, respectively. Among them, the f_{anis} is neglected for simplicity regarding the isotropic nature of the polycrystalline CoFe film. The isotropic f_{exch} is determined by the gradient of local magnetization vectors, i.e.,

$$f_{\text{exch}} = J\left[(\nabla m_1)^2 + (\nabla m_2)^2 + (\nabla m_3)^2\right], \tag{7}$$

where J denotes the exchange stiffness constant. The magnetostatic energy density f_{ms} can be written as,

$$\begin{aligned} f_{\text{ms}} &= -\frac{1}{2}\mu_0 M_S\left(\mathbf{H}_d^{\text{tot}}\cdot\mathbf{m}\right) \\ \mathbf{H}_d^{\text{tot}} &= \mathbf{H}_d^{\text{hetero}}(\mathbf{m}) + \mathbf{H}_d^{\text{shape}}(\overline{\mathbf{m}}). \end{aligned} \tag{8}$$

Here the stray field $\mathbf{H}_d^{\text{tot}}$ consists of a heterogeneous part $\mathbf{H}_d^{\text{hetero}}(\mathbf{m})$from the magnetostatic interaction which depends on local magnetization distributions and is obtained by solving magnetostatic equilibrium equation, i.e.,$\nabla\cdot\left(\mu_0\mathbf{H}_d^{\text{hetero}} + \mu_0 M_S\mathbf{m}\right)=0$, under periodic boundary conditions[42]. $\mathbf{H}_d^{\text{tot}}$ also includes an demagnetization part $\mathbf{H}_d^{\text{shape}}(\overline{\mathbf{m}})$ that relates to the average magnetization $\overline{\mathbf{m}}$ by the sample-size dependent demagnetizing factor matrix $\mathbf{N}$[43], i.e., $\mathbf{H}_d^{\text{shape}}(\overline{\mathbf{m}}) = M_S\mathbf{N}\overline{\mathbf{m}}$.

Furthermore, the $\mathbf{H}_{DM}$-field energy density can be expressed, similarly to the Zeeman energy of an external magnetic field, as,

$$f_H = -\mu_0 M_S\left(\mathbf{H}_{DM}^m\cdot\mathbf{m}\right). \tag{9}$$

The $\mathbf{H}_{DM}^m$ indicates the $\mathbf{H}_{DM}$-field imposed on the CoFe film, and is given as,

$$\mathbf{H}_{DM}^m = \frac{1}{t_i}\int_{t_i}\mathbf{H}_{DM}dz, \tag{10}$$

where t_i denotes the thickness of the interface creating interfacial magnetic interaction, and the $\mathbf{H}_{DM}$-field vector in the BFO layer can be expanded as,

$$\begin{aligned} \mathbf{H}_{DM} = \mathbf{P}\times\mathbf{L} &= h_{DM}^0\left(\frac{P_1}{|\mathbf{P}|},\frac{P_2}{|\mathbf{P}|},\frac{P_3}{|\mathbf{P}|}\right)\times\left(\frac{L_1}{|\mathbf{L}|},\frac{L_2}{|\mathbf{L}|},\frac{L_3}{|\mathbf{L}|}\right) \\ &= \frac{h_{DM}^0}{\sqrt{P_1^2+P_2^2+P_3^2}\cdot\sqrt{P_3^2(P_1^2+P_2^2)}}(P_1,P_2,P_3)\times(P_2P_3,\ -P_1P_3,\ 0) \\ &= \frac{h_{DM}^0}{\sqrt{P_1^2+P_2^2+P_3^2}\cdot\sqrt{P_3^2(P_1^2+P_2^2)}}\left(P_1P_3^2,\ P_2P_3^2,\ -P_1^2P_3-P_2^2P_3\right). \end{aligned} \tag{11}$$

The P_i and L_i (i=1,2,3) are the components of the polarization vectors and the antiferromagnetic axes along the cubic <100> axes, respectively, and the h_{DM}^0 represents the magnitude of the $\mathbf{H}_{DM}$ field that depends on the chemical composition and geometric size of a specific BFO-based heterostructure[9,44]. Note that the antiferromagnetic axis $\mathbf{L}$ is expressed as $\mathbf{L}=(P_1, P_2, 0)\times(0, 0, P_3)$, which indicates an alignment along either the in-plane $[1\bar{1}0]$ or [110] axis depending on polarization orientations (see figure 1a). Equation (11) clearly indicates that non-uniform nature of the $\mathbf{H}_{DM}$-field related to individual ferroelectric domain at the BFO surface, which can propagate across the heterointerface and act on the CoFe film similarly to the case in non-uniform ferroelastic strains ε_{ij}^{FS} [Eqs. (4a) and (4b)]. Combining Eq. (11), Eq. (10) can be rewritten as,

$$\mathbf{H}_{DM}^m = \frac{h_{DM}^0}{t_i}\int_{t_i}\frac{\left(P_1P_3^2,\ P_2P_3^2,\ -P_1^2P_3-P_2^2P_3\right)}{\sqrt{P_1^2+P_2^2+P_3^2}\cdot\sqrt{P_3^2(P_1^2+P_2^2)}}dz. \tag{12}$$

Influence of non-uniform ε_{ij}^{FS} on magnetic domain structures is characterized by changes in the elastic energy density of the CoFe, i.e., f_{elastic}^m, which can be calculated similarly to that in ferroelectric BFO [Eq. (3)] but use the elastic stiff constants of CoFe. Note these non-uniform ε_{ij}^{FS} are included in the position-dependent stress-free strain $\varepsilon_{ij}^{0-m}(\mathbf{r})$ of the magnets,

$$\varepsilon_{ij}^{0-m}(\mathbf{r}) = \begin{cases} 3/2\lambda_s\left(m_im_j - 1/3\right) + \eta\varepsilon_{ij}^{FS}(or\ \varepsilon_{ij}^{growth}),\ (i=j) \\ 3/2\lambda_s m_im_j + \eta\varepsilon_{ij}^{FS}(\text{or } \varepsilon_{ij}^{growth}),\ (i\neq j) \end{cases}, \tag{13}$$

with λ_s denoting the saturation magnetostrictive coefficient, taken as −62 ppm herein[45]. The coupling factor η ($0\le\eta\le1$) is introduced to describe the possible loss of transferred strain due to imperfect interface contact, and is assumed to be 1 for a full strain transfer.

Temporal evolutions of the ferroelectric and magnetic domain structures are obtained by numerically solving the TDGL and LLG equations using semi-implicit Fourier spectral method[46] and Gauss-Seidel projection method[47], respectively. The material parameters used for simulations, including the Landau coefficients, electrostrictive coefficients, elastic constants, gradient energy coefficients of BFO layer, and the saturated magnetization, exchange stiffness constant, elastic constants of CoFe layer, are taken from literatures[48–50]. The discrete grid points of $128\Delta x\times128\Delta y\times48\Delta z$ with real grid space $\Delta x=\Delta y=10$ nm, and $\Delta z=4$ nm are employed to describe the BFO film/substrate system, wherein the thickness of BFO t_p is taken as 112 nm by setting $t_p=28\Delta z$, and the thickness of the interface t_i creating the interfacial magnetic interaction is taken as 4 nm by setting $t_i=1\Delta z$. While for CoFe thin film, discrete grid points of $128\Delta x\times128\Delta y\times20\Delta z$ with $\Delta x=\Delta y=10$ nm, and $\Delta z=0.5$ nm are used, where the thickness of the CoFe t_m is set to be 2. 5 nm by taking $t_m=5\Delta z$.

1. Chu, Y.-H. *et al.* Electric-field control of local ferromagnetism using a magnetoelectric multiferroic. *Nat. Mater.* **7**, 478–482 (2008).
2. Heron, J. *et al.* Electric-field-induced magnetization reversal in a ferromagnet-multiferroic heterostructure. *Phys. Rev. Lett.* **107**, 217202 (2011).
3. Wu, S. M. *et al.* Reversible electric control of exchange bias in a multiferroic field-effect device. *Nat. Mater* **9**, 756–761.
4. Wu, S. M. *et al.* Full electric control of exchange Bias. *Phys. Rev. Lett.* **110**, 067202 (2013).
5. Mathur, N. Materials science: A desirable wind up. *Nature* **454**, 591 (2008).
6. Zeches, R. J. *et al.* A strain-driven morphotropic phase boundary in $BiFeO_3$. *Science* **326**, 977 (2009).
7. Zhang, J. X. *et al.* Large field-induced strains in a lead-free piezoelectric material *Nat. Nano.* **6**, 98 (2011).
8. Chu, Y.-H. *et al.* Nanoscale control of domain architectures in $BiFeO_3$ thin films. *Nano lett.* **9**, 1726 (2009).
9. Trassin, M. *et al.* Interfacial coupling in multiferroic/ferromagnet heterostructures. *Phys. Rev. B* **87**, 134426 (2013).
10. Dzyaloshinskii, I. Thermodynamic theory of weak ferromagnetism in antiferromagnetic substances. *Sov. Phys. JETP* **5**, 1259 (1957).

11. Moriya, T. Anisotropic superexchange interaction and weak ferromagnetism. *Phys. Rev.* **120**, 91 (1960).
12. Ederer, C. & Spaldin, N. A. Weak ferromagnetism and magnetoelectric coupling in bismuth ferrite. *Phys. Rev. B* **71**, 060401 (2005).
13. Ederer, C. & Fennie, C. J. Electric-field switchable magnetization via the Dzyaloshinskii–Moriya interaction: $FeTiO_3$ versus $BiFeO_3$. *J. Phys.: Condens. Matter* **20**, 434219 (2008).
14. Holcomb, M. *et al.* Probing the evolution of antiferromagnetism in multiferroics. *Phys. Rev. B* **81**, 134406 (2010).
15. Infante, I. C. *et al.* Bridging multiferroic phase transitions by epitaxial strain in $BiFeO_3$. *Phys. Rev. Lett.* **105**, 057601 (2010).
16. Sando, D. *et al.* Crafting the magnonic and spintronic response of $BiFeO_3$ films by epitaxial strain. *Nat. Mater.* **12**, 641 (2013).
17. Hu, J.-M., Sheng, G., Zhang, J., Nan, C. W. & Chen, L. Phase-field simulation of strain-induced domain switching in magnetic thin films. *Appl. Phys. Lett.* **98**, 112505 (2011).
18. Lahtinen, T. H., Tuomi, J. O. & van Dijken, S. Pattern transfer and electric-field-induced magnetic domain formation in multiferroic heterostructures. *Adv. Mater.* **23**, 3187 (2011).
19. Lahtinen, T. H., Franke, K. J. & van Dijken, S. Electric-field control of magnetic domain wall motion and local magnetization reversal. *Sci. Rep.* **2**, 258 (2012).
20. Lahtinen, T. H. *et al.* Alternating domains with uniaxial and biaxial magnetic anisotropy in epitaxial Fe films on $BaTiO_3$. *Appl. Phys. Lett.* **101**, 262405 (2012).
21. Chopdekar, R. *et al.* Spatially resolved strain-imprinted magnetic states in an artificial multiferroic. *Phys. Rev. B* **86**, 014408 (2012).
22. Lahtinen, T. H. & van Dijken, S. Temperature control of local magnetic anisotropy in multiferroic CoFe/$BaTiO_3$. *Appl. Phys. Lett.* **102**, 112406 (2013).
23. Chen, L.-Q. Phase-field models for microstructure evolution. *Annu. Rev. Mater. Res.* **32**, 113 (2002).
24. Chen, L. Q. Phase-Field method of phase transitions/domain structures in ferroelectric thin films: A Review. *J. Am. Ceram. Soc.* **91**, 1835 (2008).
25. Hu, J.-M., Li, Z., Chen, L.-Q. & Nan, C.-W. High-density magnetoresistive random access memory operating at ultralow voltage at room temperature. *Nat. Comm.* **2**, 553 (2011).
26. Hu, J. M., Li, Z., Chen, L. Q. & Nan, C. W. Design of a voltage-controlled magnetic random access memory based on anisotropic magnetoresistance in a single magnetic layer. *Adv. Mater.* **24**, 2869 (2012).
27. Hu, J. M. *et al.* Film size-dependent voltage-modulated magnetism in multiferroic heterostructures. *Philos. Trans. A* **372**, 20120444 (2014).
28. Duan, C.-G. *et al.* Surface magnetoelectric effect in ferromagnetic metal films. *Phys. Rev. Lett.* **101**, 137201 (2008).
29. Rondinelli, J. M., Stengel, M. & Spaldin, N. A. Carrier-mediated magnetoelectricity in complex oxide heterostructures. *Nat. Nanotechnol.* **3**, 46–50 (2008).
30. Duan, C.-G., Jaswal, S. S. & Tsymbal, E. Y. Predicted magnetoelectric effect in Fe/$BaTiO_3$ multilayers: ferroelectric control of magnetism. *Phys. Rev. Lett.* **97**, 047201 (2006).
31. Garcia, V. *et al.* Ferroelectric control of spin polarization. *Science* **327**, 1106–1110 (2010).
32. Hu, J.-M., Nan, C.-W. & Chen, L.-Q. Size-dependent electric voltage controlled magnetic anisotropy in multiferroic heterostructures: Interface-charge and strain comediated magnetoelectric coupling. *Phys. Rev. B* **83**, 134408 (2011).
33. Hu, J.-M., Yang, T., Chen, L. & Nan, C. W. Voltage-driven perpendicular magnetic domain switching in multiferroic nanoislands. *J. Appl. Phys.* **113**, 194301 (2013).
34. Nambu, S. & Sagala, D. A. Domain formation and elastic long-range interaction in ferroelectric perovskites. *Phy. Rev. B* **50**, 5838 (1994).
35. Zhang, J. *et al.* Computer simulation of ferroelectric domain structures in epitaxial $BiFeO_3$ thin films. *J. Appl. Phys.* **103**, 094111 (2008).
36. Li, Y., Hu, S., Liu, Z. & Chen, L. Effect of electrical boundary conditions on ferroelectric domain structures in thin films. *Appl. Phys. Lett.* **81**, 427 (2002).
37. Khachaturyan, A. *Theory of structural transfomations in solid.* (Wiley, 1983).
38. Hu, J.-M. & Nan, C. W. Electric-field-induced magnetic easy-axis reorientation in ferromagnetic/ferroelectric layered heterostructures. *Phys. Rev. B* **80**, 224416 (2009).
39. Chu, Y. H. *et al.* Nanoscale domain control in multiferroic $BiFeO_3$ thin films. *Adv. Mater.* **18**, 2307–2311 (2006).
40. Walowski, J. *et al.* Intrinsic and non-local Gilbert damping in polycrystalline nickel studied by Ti : sapphire laser fs spectroscopy. *J. Phys. D: Appl. Phys.* **41**, 164016 (2008).
41. Qiu, D., Ashraf, K. & Salahuddin, S. Nature of magnetic domains in an exchange coupled $BiFeO_3$/CoFe heterostructure. *Appl. Phys. Lett.* **102**, 112902 (2013).
42. Zhang, J. & Chen, L. Phase-field microelasticity theory and micromagnetic simulations of domain structures in giant magnetostrictive materials. *Acta Mater.* **53**, 2845 (2005).
43. Aharoni, A. Demagnetizing factors for rectangular ferromagnetic prisms. *J. Appl. Phys.* **83**, 3432 (1998).
44. Huijben, M. *et al.* Ultrathin limit of exchange bias coupling at oxide multiferroic/ferromagnetic interfaces. *Adv. Mater.* **25**, 4739–4745 (2013).
45. Cullity, B. D. & Graham, C. D. *Introduction to Magnetic Materials, 2nd ed.,* page 253 (Wiley, 2009).
46. Chen, L. & Shen, J. Applications of semi-implicit Fourier-spectral method to phase field equations. *Comput. Phys. Comm.* **108**, 147 (1998).
47. Wang, X. P., Garcia-Cervera, C. J. & Weinan, E. A Gauss-Seidel projection method for micromagnetics simulations. *J. Comput. Phys.* **171**, 357, doi:10.1006/jcph.2001.6793 (2001).
48. Hu, J.-M. *et al.* A simple bilayered magnetoelectric random access memory cell based on electric-field controllable domain structure. *J. Appl. Phys.* **108**, 043909 (2010).
49. Streubel, R., Köhler, D., Schäfer, R. & Eng, L. M. Strain-mediated elastic coupling in magnetoelectric nickel/barium-titanate heterostructures. *Phys. Rev. B* **87**, 054410 (2013).
50. Zhang, J. *et al.* Effect of substrate-induced strains on the spontaneous polarization of epitaxial $BiFeO_3$ thin films. *J. Appl. Phys.* **101**, 114105 (2007).

Acknowledgments

This work is supported by the NSF of China (Grant Nos. 51332001, 11234005 and 51221291), Beijing Education Committee (Grant No. 20121000301), and the NSF under grant No DMR-1006541.

Author contributions

J.J.W., J.M.H. and T.Y. performed the simulations. C.W.N. and L.Q.C. directed the work. J.M.H., J.J.W., L.Q.C. and C.W.N. co-wrote the paper. J.J.W., J.M.H., M.F., J.Z. and C.W.N. analyzed the data. All contributed discussion.

Additional information

Supplementary information accompanies this paper at http://www.nature.com/scientificreports

Competing financial interests: The authors declare no competing financial interests.

How to cite this article: Wang, J.J. *et al.* Effect of strain on voltage-controlled magnetism in $BiFeO_3$-based heterostructures. *Sci. Rep.* **4**, 4553; DOI:10.1038/srep04553 (2014).